VOLUME 14 No. 1, 22 December 2024 Pages 29-42

MALE UAV LONGITUDINAL STABILITY DETERMINATION USING WIND TUNNEL DATA

PENENTUAN KESTABILAN LONGITUDINAL PESAWAT NIRAWAK MALE MENGGUNAKAN DATA TEROWONGAN ANGIN

Muhammad Ilham Adhynugraha and Fadly Cahya Megawanto
Research Center for Aeronautics Technology, National Research and Innovation Agency

Siti Vivi Octaviany
Research Center for Transportation, National Research and Innovation Agency

Dewi Habsari Budiarti* and Jemie Muliadi
Research Center for Artificial Intelligence and Cyber Security, National Research and Innovation Agency

Osen Fili Nami
Research Center for Electronics, National Research and Innovation Agency

Singgih Satrio Wibowo
Mechanical Engineering, Politeknik Negeri Bandung

Submitted: 2023-09-30; Revised: 2024-11-01; Accepted:2024-11-09

ABSTRAK

Sistem udara tanpa awak semakin diminati untuk berbagai operasi, dan juga peningkatan teknologi sistem navigasi dan komunikasi yang sangat cepat. Salah satu hal terpenting dalam merancang sistem udara tanpa awak adalah memastikan kestabilan sistem, seperti kestabilan longitudinal. Studi ini dilakukan untuk pesawat Unmanned Aerial System (UAS) Medium Altitude Long Endurace (MALE). Fokusnya adalah menganalisis stabilitas longitudinal MALE UAS. Pendekatan matematika dilakukan untuk menganalisis kestabilan longitudinal UAS. Serangkaian uji terowongan angin menggunakan model berskala dari MALE UAS dilakukan untuk menghasilkan beberapa set data yang berisi koefisien turunan kestabilan yang diperlukan. Koefisien turunan kestabilan ini digunakan untuk menntukan karakteristik gerakan longitudinal pesawat. Analisis koefisien turunan kestabilan serta mode phugoid dan periode pendek menunjukkan bahwa pesawat stabil secara statis dan dinamis dalam gerak longitudinal. Hasilnya menunjukkan perubahan berat mengakibatkan perubahan frekuensi alami mode periode pendek. Responsnya juga memerlukan waktu yang lebih lama untuk mencapai keadaan keseimbangan kembali setelah terjadi gangguan. Waktu yang diperlukan untuk meredam osilasi pada kecepatan aksial dan normal adalah lebih dari 100 detik. Untuk respon pitch rate dan sudut pitch, kestabilan dicapai dalam waktu sekitar 65 detik.

Keywords: *Turunan Koefisien Aerodinamika; Gerak Longitudinal; MALE; Kestabilan; PUNA*

*Corresponding author: dewi037@brin.go.id

ABSTRACT

Unmanned aerial systems have been increasing in demand for a wide range of operations, including the rapid growth of advanced navigation and communication. One of the most important things in designing an Unmanned Aerial System (UAS) is to ensure the system's stability, such as the UAS itself. This study was conducted on an in-house medium altitude long endurance (MALE) UAS aircraft. It is focused on analyzing the longitudinal stability of MALE UAS. A mathematical approach was used to analyze the longitudinal stability. A series of wind tunnel tests using a scaled model of the MALE UAS is done to produce several sets of data containing longitudinal stability derivatives for various configurations. A few sets of data are chosen to obtain the stability derivatives needed. These stability derivatives are utilized to determine the longitudinal motion characteristic of the aircraft. The analysis of certain derivatives and the phugoid and short-period mode shows that the aircraft is statically and dynamically stable in longitudinal motion. The results indicated that a weight change prompted an altercation in the natural frequency of the short-period mode. The response also showed that reaching a new equilibrium state takes a rather long period after an arbitrary perturbation is initiated. The time required to subdue oscillation in axial and average velocities is more than 100 seconds. The stability in the pitch rate is reached in around 65 seconds. The time to reach stability in pitch angle response is around 65 seconds.

Keywords: *Aerodynamics Derivatives; Longitudinal Motion; MALE; Stability; UAS*

INTRODUCTION

Unmanned aerial systems (UAS) have been increasing in demand for a wide range of operations. The rise of interest in this technology is linked to the rapid growth of advanced navigation and communication fields. The UAS terminology represents the shift of importance from the aircraft to the whole vehicle system, including ground control systems (GCS) and data links. The missions that UAS can carry out are vast, ranging both for civilian and military purposes. The sort of missions include photogrammetry and remote sensing (Colomina & Molina, 2014), surveillance and monitoring (Li & Savkin, 2021), cargo (Taylor, 2010), reconnaissance (Stodola et al., 2019), and even combatant (Gertler, 2012). Application-wise, a particular mission will determine the design of UAS.

An in-house UAS project was designed for medium altitude and long endurance (MALE) operation. These features have been chosen to meet the requirements for intelligence, surveillance, and reconnaissance missions. One concern to be aware of is the stability of the unmanned aerial vehicle (UAV), which is one of the main components in designing the control law of the whole system.

Upon the development of the vehicle, several approaches to designing MALE UAVs have been studied thoroughly by (Iqbal et al., 2008; Iqbal & Sullivan, 2009; Panagiotou et al., 2016; Pericles Panagiotou et al., 2018) amongst others, employ tools of high fidelity of computer-aided design (CAD), computational fluid dynamics (CFD), and finite element method (FEM). Some of these approaches have also been applied to the project. The design for further consideration has been through a series of wind tunnel tests providing an aerodynamic data set. This data set is employed to provide stability derivatives of the vehicle as a foundation to develop the vehicle's control system.

Figure 1.
Perspective illustration of the UAV
Source: Research Centre for Aeronautics Technology (BRIN) (2021)

The use of wind tunnel data to determine the stability of aircraft has been a conventional approach, but its reliability is still relevant for today's application. One example of this approach is presented by (Panagiotou et al., 2018) over a new design of turboprop passenger aircraft. As the first finding

shows an insufficient stability characteristic, an attempt at design improvement can be considered, and a study can be carried out to determine the flight performance and characteristics of Otto Lilienthal's glider through wind tunnel experimentation. The wind tunnel results give a better understanding of the aerodynamic and stability characteristics of the historical glider, including the significance of fabric selection towards the design.

For the UAV study, one example is shown by (Wienke et al., 2021) in determining the stability characteristics of a morphing wing UAV. Wind tunnel data helped model validation for lateral-directional motion with the influence of variable aspect ratio (VAR). More recently, (Henry et al., 2005) presented the significance of wind tunnel experiments on a small delta-wing UAV to determine its static stability derivatives, control derivatives, damping derivatives, and thrust model.

The novelty of this research lies in the combination of wind tunnel experiments and mathematical analysis to determine the longitudinal stability of MALE-type UAVs with a weight above 500 kg. Unlike prior studies that primarily relied on numerical simulations (Adeleke, et al., 2022) or limited scale-model testing, this research integrates experimental wind tunnel data with theoretical analysis to obtain longitudinal stability derivatives. The study also reveals the impact of weight changes on the natural frequency of the short-period mode, offering new insights into how weight variations influence the aircraft's dynamic response. This research provides an essential contribution by highlighting how these findings can improve the design of UAV control systems and ensure mission success.

METHOD

Mathematical Approach

The UAV is a rigid body in space with 6 degrees of freedom. In the frame of small-disturbance theory, the linearized equations of motion are described in the set of equations (1) (Cook, 2007).

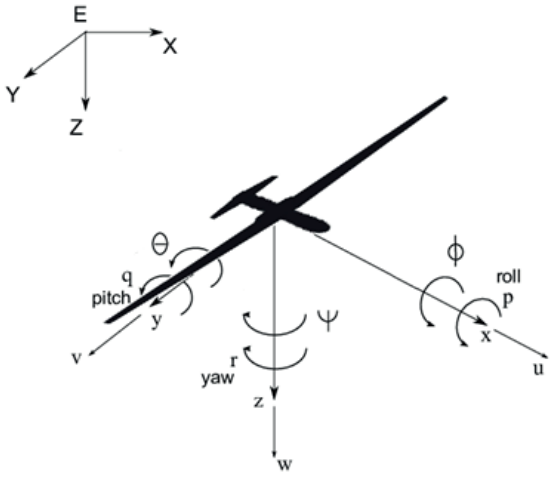

Figure 2.
Illustration of 6 DOF of a UAV
Source: Research Centre for Aeronautics Technology (BRIN) (2021)

$$m(\dot{u} + qW_e) = X_{a_e} + \mathbb{X}_u u + \mathbb{X}_v v + \mathbb{X}_w w + \mathbb{X}_p p + \mathbb{X}_q q + \mathbb{X}_r r + \mathbb{X}_{\dot{w}} \dot{w} - mg \sin\theta_e - mg\theta \cos\theta_e + \mathbb{X}_\xi \xi + \mathbb{X}_\eta \eta + \mathbb{X}_\varsigma \varsigma + \mathbb{X}_\tau \tau$$

$$m(\dot{v} - pW_e + rU_e) = Y_{a_e} + \mathbb{Y}_u u + \mathbb{Y}_v v + \mathbb{Y}_w w + \mathbb{Y}_p p + \mathbb{Y}_q q + \mathbb{Y}_r r + \mathbb{Y}_{\dot{w}} \dot{w} + mg\psi \sin\theta_e + mg\phi \cos\theta_e + \mathbb{Y}_\xi \xi + \mathbb{Y}_\eta \eta + \mathbb{Y}_\varsigma \varsigma + \mathbb{Y}_\tau \tau$$

$$m(\dot{w} - qU_e) = Z_{a_e} + \mathbb{Z}_u u + \mathbb{Z}_v v + \mathbb{Z}_w w + \mathbb{Z}_p p + \mathbb{Z}_q q + \mathbb{Z}_r r + \mathbb{Z}_{\dot{w}} \dot{w} + mg \cos\theta_e - mg\theta \sin\theta_e + \mathbb{Z}_\xi \xi + \mathbb{Z}_\eta \eta + \mathbb{Z}_\varsigma \varsigma + \mathbb{Z}_\tau \tau$$

$$I_x \dot{p} - I_{xz} \dot{r} = L_{a_e} + \mathbb{L}_u u + \mathbb{L}_v v + \mathbb{L}_w w + \mathbb{L}_p p + \mathbb{L}_q q + \mathbb{L}_r r + \mathbb{L}_{\dot{w}} \dot{w} + \mathbb{L}_\xi \xi + \mathbb{L}_\eta \eta + \mathbb{L}_\varsigma \varsigma + \mathbb{L}_\tau \tau$$

$$I_y \dot{q} = M_{a_e} + \mathbb{M}_u u + \mathbb{M}_v v + \mathbb{M}_w w + \mathbb{M}_p p + \mathbb{M}_q q + \mathbb{M}_r r + \mathbb{M}_{\dot{w}} \dot{w} + \mathbb{M}_\xi \xi + \mathbb{M}_\eta \eta + \mathbb{M}_\varsigma \varsigma + \mathbb{M}_\tau$$

$$I_z \dot{r} - I_{xz} \dot{p} = N_{a_e} + \mathbb{N}_u u + \mathbb{N}_v v + \mathbb{N}_w w + \mathbb{N}_p p + \mathbb{N}_q q + \mathbb{N}_r r + \mathbb{N}_{\dot{w}} \dot{w} + \mathbb{N}_\xi \xi + \mathbb{N}_\eta \eta + \mathbb{N}_\varsigma \varsigma + \mathbb{N}_\tau \tau$$

(1) The Linearized Equations of Motion

Table 1. Symbol definition

Symbol	Definition	Symbol	Definition
$\mathbf{A}$	State matrix of the state equation in state space form	u	Axial velocity perturbation; used also in subscript
$\mathbf{A}_{ph}$	State matrix of the state equation in state space form for the phugoid mode	$\mathbf{u}$	Input vector of the state equation in state space form
$\mathbf{A}_{sp}$	State matrix of the state equation in state space form for short period mode	U_e	The axial component of steady equilibrium velocity
$\mathbf{B}$	Input matrix of the state equation in state space form	v	Lateral velocity perturbation; used also in subscript
$\mathbf{B}_{ph}$	Input matrix of the state equation in state space form for the phugoid mode	w	Normal velocity perturbation; used also in subscript
$\mathbf{B}_{sp}$	Input matrix of the state equation in state space form for the short period mode	W_e	The normal component of steady equilibrium velocity
$\mathbf{C}$	Output matrix of the output equation in state space form	$\mathbf{x}$	State vector of the state equation in state space form
$\mathbf{D}$	Direct matrix of the output equation in state space form	x_i	Aerodynamic stability derivative of axial force divided by appropriate mass or inertia due to parameter i
g	Acceleration due to gravity	X_{a_e}	Aerodynamic axial force at steady condition
$\mathbf{I}$	Identity matrix		
I_x	Moment inertia in roll	$\mathbb{X}_i$	Dimensional stability derivative of axial force due to parameter *i*; in dimensionless denoted as
I_y	Moment inertia in pitch	$\mathbf{y}$	Output vector of the output equation in state space form
I_z	Moment inertia in yaw	y_i	Aerodynamic stability derivative of lateral force divided by appropriate mass or inertia due to parameter *i*
I_{xy}	Product of inertia about x- and y-planes	Y_{a_e}	Aerodynamic lateral force at steady condition
I_{xz}	Product of inertia about x- and z-planes	$\mathbb{Y}_i$	Dimensional stability derivative of lateral force due to parameter *i*; in dimensionless denoted as
I_{yz}	Product of inertia about y- and z-planes	z_i	Aerodynamic stability derivative of normal force divided by appropriate mass or inertia due to parameter *i*
m	Mass	Z_{a_e}	Aerodynamic normal force at steady condition
L_{a_e}	Aerodynamic rolling moment at steady condition	$\mathbb{Z}_i$	Dimensional stability derivative of normal force due to parameter *i*; in dimensionless denoted as
$\mathbb{L}_i$	Dimensional stability derivative of rolling moment due to parameter *i;* in dimensionless denoted as	η	Elevator angle perturbation; used also in subscript
M_{a_e}	Aerodynamic pitching moment at steady condition	θ	Pitch angle perturbation; used also in subscript

Symbol	Definition	Symbol	Definition
$\mathbb{M}_i$	Dimensional stability derivative of pitching moment due to parameter *i;* in dimensionless denoted as	θ_e	Equilibrium pitch angle
N_{a_e}	Aerodynamic yawing moment at steady condition	ξ	Aileron angle perturbation
$\mathbb{N}_i$	Dimensional stability derivative of the yawing moment due to parameter *i*; in dimensionless denoted as	ς	Rudder angle perturbation
p	Roll rate perturbation; used also in subscript	ς_{ph}	Phugoid damping ratio
q	Pitch rate perturbation; used also in subscript	ς_{sp}	Short period damping ratio
r	Yaw rate perturbation; used also in subscript	τ	Engine thrust perturbation
s	Laplace operator	ω_{ph}	Phugoid undamped natural frequency
t	Time	ω_{sp}	Short period undamped natural frequency

Source: Author's Documentation (2024)

As the current study limits the discussion of longitudinal motion only, the set of equations above can be constrained to the longitudinal plane. Hence, the motion is described only by the axial force, the normal force, and the pitching moment. Note this point of view: the lateral-longitudinal coupling is considered negligible, and the effect of the rudder and aileron is minimal. Meanwhile, in the trim condition, the steady state gives:

$$X_{a_e} = mg \sin\theta_e$$
$$Y_{a_e} = 0$$
$$Z_{a_e} = -mg \cos\theta_e$$
$$L_{a_e} = 0$$
$$M_{a_e} = 0$$
$$N_{a_e} = 0$$

(2) Steady State Condition

Taking into account all the simplification above-mentioned, the set of equations (1) may be written as follows:

$$m\dot{u} - \mathbb{X}_u u - \mathbb{X}_w w - \mathbb{X}_{\dot{w}}\dot{w} - \left(\mathbb{X}_q - mW_e\right)q + mg\theta\cos\theta_e = \mathbb{X}_\eta\eta + \mathbb{X}_\tau\tau$$
$$-\mathbb{Z}_u u - \mathbb{Z}_w w + (m - \mathbb{Z}_{\dot{w}})\dot{w} - \left(\mathbb{Z}_q + mU_e\right)q + mg\theta\sin\theta_e = \mathbb{Z}_\eta\eta + \mathbb{Z}_\tau\tau$$
$$-\mathbb{M}_u u - \mathbb{M}_w w - \mathbb{M}_{\dot{w}}\dot{w} + I_y\dot{q} - \mathbb{M}_q q = \mathbb{M}_\eta\eta + \mathbb{M}_\tau\tau$$

(3) The Linearized Equations of Motion after Simplification

During operation in level flight thus, the reference axes are wind or stability axes; it is convenient to settle that the:

$$\theta_e = W_e = 0$$

(4) Level Flight

And the equations (3) can be simplified even further to:

$$m\dot{u} - \mathbb{X}_u u - \mathbb{X}_w w - \mathbb{X}_{\dot{w}}\dot{w} - \mathbb{X}_q q + mg\theta = \mathbb{X}_\eta \eta + \mathbb{X}_\tau \tau$$
$$-\mathbb{Z}_u u - \mathbb{Z}_w w + (m - \mathbb{Z}_{\dot{w}})\dot{w} - (\mathbb{Z}_q + mU_e)q = \mathbb{Z}_\eta \eta + \mathbb{Z}_\tau \tau$$
$$-\mathbb{M}_u u - \mathbb{M}_w w - \mathbb{M}_{\dot{w}}\dot{w} + I_y \dot{q} - \mathbb{M}_q q = \mathbb{M}_\eta \eta + \mathbb{M}_\tau \tau$$

(5) Simplified Linearized Equations of Motion

The script letters $\mathbb{X}_i$, $\mathbb{Z}_i$, and $\mathbb{M}_i$ represent the dimensional longitudinal aerodynamic stability derivatives due to parameter i. Taking suitable multipliers, these derivatives can be changed into dimensionless values presented in $X_{i'}$ $Z_{i'}$ and M_i . Further description of these derivatives is available in (O'Donnell & Mohseni 2018).

The motion of the UAV can be described in a multidimensional vector space, and the set of equations of motion may be rewritten into a state equation of the linear time-invariant (LTI) with a complement of the output equation to determine the system output variables. Both equations are written as follows,

$$\dot{\mathbf{x}}(t) = \mathbf{A}\mathbf{x}(t) + \mathbf{B}\mathbf{u}(t)$$
$$\mathbf{y}(t) = \mathbf{C}\mathbf{x}(t) + \mathbf{D}\mathbf{u}(t)$$

(6) State Space Equation Form

When the equations (5) are transformed into a relationship similar to the state equation, we obtain

$$\mathbf{M}\dot{\mathbf{x}}(t) = \mathbf{A}'\mathbf{x}(t) + \mathbf{B}'\mathbf{u}(t)$$

(7) Linearized Equation of Motion

Where:

$$\mathbf{x}^{\boldsymbol{T}}(\mathbf{t}) = (u \quad w \quad q \quad \theta);$$

$$\mathbf{u}^{\boldsymbol{T}}(\mathbf{t}) = (\eta \quad \tau)$$

$$\mathbf{M} = \begin{bmatrix} m & -\mathbb{X}_{\dot{w}} & 0 & 0 \\ 0 & (m - \mathbb{Z}_{\dot{w}}) & 0 & 0 \\ 0 & -\mathbb{M}_{\dot{w}} & I_y & 0 \\ 0 & 0 & 0 & 1 \end{bmatrix}$$

$$\mathbf{A}' = \begin{bmatrix} \mathbb{X}_u & \mathbb{X}_w & \mathbb{X}_q & -mg \\ \mathbb{Z}_u & \mathbb{Z}_w & (\mathbb{Z}_q + mU_e) & 0 \\ \mathbb{M}_u & \mathbb{M}_w & \mathbb{M}_q & 0 \\ 0 & 0 & 1 & 0 \end{bmatrix};$$

$$\mathbf{B}' = \begin{bmatrix} \mathbb{X}_\eta & \mathbb{X}_\tau \\ \mathbb{Z}_\eta & \mathbb{Z}_\tau \\ \mathbb{M}_\eta & \mathbb{M}_\tau \\ 0 & 0 \end{bmatrix}$$

$$\dot{\theta} = q$$

The system in equation (7) is not in the state space form yet and thus needs further treatment which fits the following relationship,

$$\dot{\mathbf{x}}(t) = \mathbf{M}^{-1}\mathbf{A}'\mathbf{x}(t) + \mathbf{M}^{-1}\mathbf{B}'\mathbf{u}(t)$$

(8) Linearized Equation of Motion in the State Equation form

Where:

$$\mathbf{M}^{-1}\mathbf{A}' = \mathbf{A} = \begin{bmatrix} x_u & x_w & x_q & x_\theta \\ z_u & z_w & z_q & z_\theta \\ m_u & m_w & m_q & m_\theta \\ 0 & 0 & 1 & 0 \end{bmatrix};$$

$$\mathbf{M}^{-1}\mathbf{B}' = \mathbf{B} = \begin{bmatrix} x_\eta & x_\tau \\ z_\eta & z_\tau \\ m_\eta & m_\tau \\ 0 & 0 \end{bmatrix}$$

Thus, the state equation becomes

$$\begin{bmatrix}\dot{u}\\ \dot{w}\\ \dot{q}\\ \dot{\theta}\end{bmatrix}=\begin{bmatrix}x_u & x_w & x_q & x_\theta\\ z_u & z_w & z_q & z_\theta\\ m_u & m_w & m_q & m_\theta\\ 0 & 0 & 1 & 0\end{bmatrix}\begin{bmatrix}u\\ w\\ q\\ \theta\end{bmatrix}+\begin{bmatrix}x_\eta & x_\tau\\ z_\eta & z_\tau\\ m_\eta & m_\tau\\ 0 & 0\end{bmatrix}\begin{bmatrix}\eta\\ \tau\end{bmatrix}$$

(9) Linearized Equation of Motion in the State Equation form

As for the output equation, it is favourable to select the output variables to be the state variables, giving the latter part of the set of equations (6) becomes

$$\mathbf{y}(t)=\mathbf{x}(t) \tag{10}$$

Thus, is an identity matrix and is a zero matrix. Following this condition, it can be obtained that

$$\mathbf{y}(t)=\mathbf{I}\mathbf{x}(t)=\begin{bmatrix}1 & 0 & 0 & 0\\ 0 & 1 & 0 & 0\\ 0 & 0 & 1 & 0\\ 0 & 0 & 0 & 1\end{bmatrix}\begin{bmatrix}u\\ w\\ q\\ \theta\end{bmatrix} \tag{11}$$

The longitudinal dynamic stability is mainly described in two modes, i.e. the short period and phugoid modes. These modes can be analyzed separately to simplify the problem. The short period pitching oscillation is influenced primarily by the average velocity and pitch rate. Conversely, the phugoid oscillation is affected by the axial velocity and pitch angle. With the trim condition applied, hence the reduced order of equation (9) for phugoid oscillation can be rewritten into

$$\begin{bmatrix}\dot{u}\\ \dot{\theta}\end{bmatrix}=\begin{bmatrix}x_u-x_w\left(\dfrac{m_uU_e-m_qz_u}{m_wU_e-m_qz_w}\right) & -g\\ \dfrac{m_uz_w-m_wz_u}{m_wU_e-m_qz_w} & 0\end{bmatrix}\begin{bmatrix}u\\ \theta\end{bmatrix}+\begin{bmatrix}x_\eta-x_w\left(\dfrac{m_\eta U_e-m_qz_\eta}{m_wU_e-m_qz_w}\right)\\ \dfrac{m_\eta z_w-m_wz_\eta}{m_wU_e-m_qz_w}\end{bmatrix}\eta$$

(12) Phugoid Oscillation

For the short-period mode, the reduced-order equation

$$\begin{bmatrix}\dot{w}\\ \dot{q}\end{bmatrix}=\begin{bmatrix}z_w & z_q\\ m_w & m_q\end{bmatrix}\begin{bmatrix}w\\ q\end{bmatrix}+\begin{bmatrix}z_\eta\\ m_\eta\end{bmatrix}\eta$$

(13) Short Period Mode

The characteristic equations above are more useful to be written in Laplace transformation, which is generally written as:

$$\boldsymbol{\Delta}(\mathrm{s})=\det[s\mathbf{I}-\mathbf{A}]=0$$

(14) Laplace Transformation

$$\boldsymbol{\Delta}(\mathrm{s})=s^2+2\varsigma_{ph}\omega_{ph}s+{\omega_{ph}}^2$$

(15) Laplace Transformation for Phugoid Mode

$$\boldsymbol{\Delta}(\mathrm{s})=s^2+2\varsigma_{sp}\omega_{sp}s+{\omega_{sp}}^2$$

(16) Laplace Transformation for Short period Mode

Data Acquisition

The determination of longitudinal motion was limited in the maximum cruise condition at an altitude of 16,000 ft with two variable weights. This restriction was considered to obtain the characteristic of the medium altitude of the vehicle and depicts the weight change due to the operation. Also, the effect of engine thrust perturbation was not considered in this study due to the assumption of trim condition. The acquired wind tunnel data was processed to produce longitudinal aerodynamic stability derivatives, as shown

in Table 2. In contrast, the setup of the MALE model in the wind tunnel can be seen in Figure 3. The testing method in the wind tunnel can be looked at explicitly (Purwadi, 2019). Wind tunnel testing for this MALE model utilizes the Indonesian Low-Speed Tunnel (ILST). The specifics of ILST can be found in (Sakya, et al., 1998) and (Hasim, F. et al., 2008). Many research works were done using ILST, such as, (Purwadi, P. et al., 2023), (Soemaryanto, et al., 2023), and (Adhynugraha, et al., 2023)

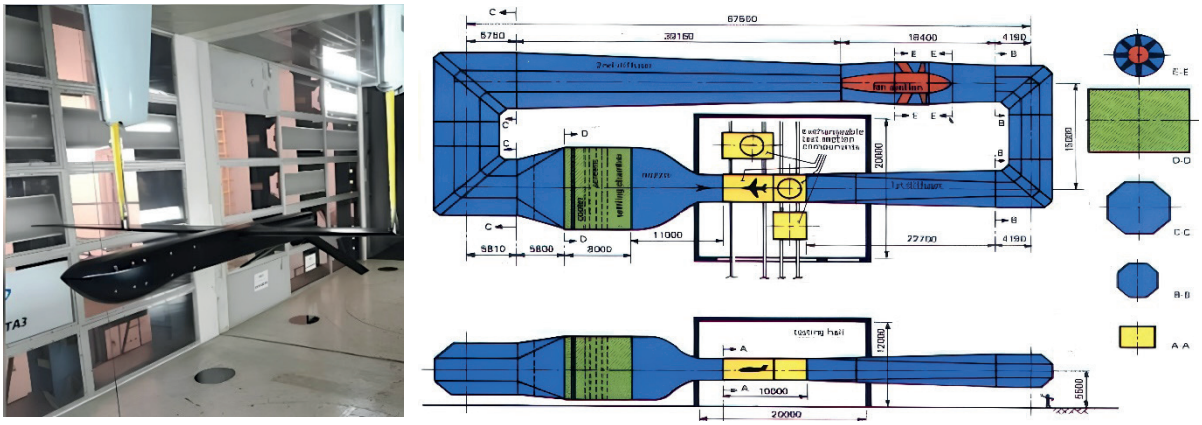

Figure 3.
The Wind Tunnel Testing
Source: Author's Documentation (2024)

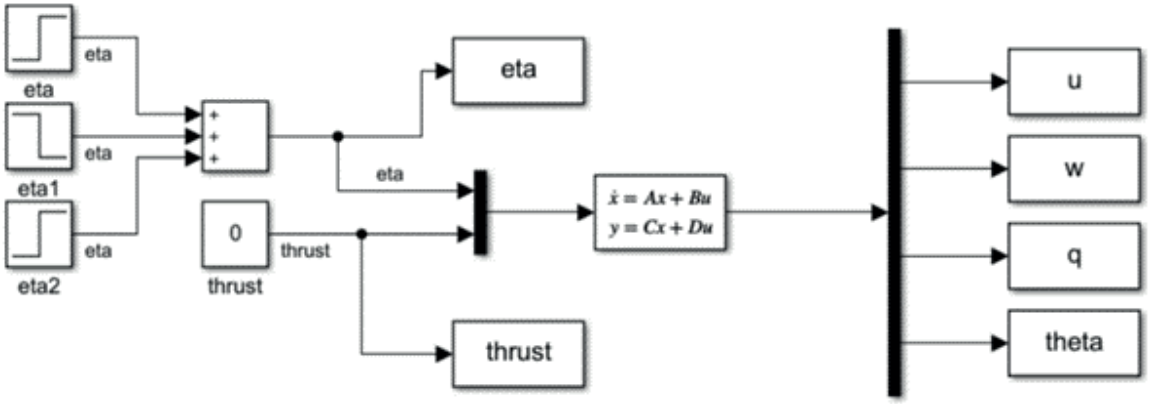

Figure 4.
State Space Block Diagram
Source: Author's Documentation (2024)

The derivatives were input into a state space block and run in the Simulink platform. The state space block is shown in Figure 4. An arbitrary small perturbation was introduced to the system by exciting a doublet to the elevator (Figure 5). The results were then analyzed further to determine the longitudinal motion characteristic of the UAV.

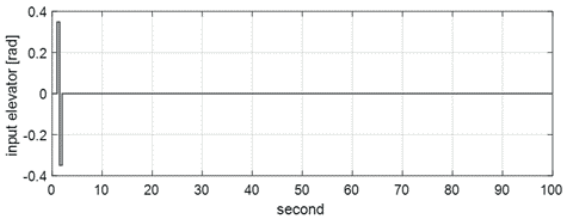

Figure 5.
Arbitrary Perturbation Input
Source: Author's Documentation (2024)

Table 2.
Dynamic stability derivatives in longitudinal motion

Alt. (ft)	Wgt. #1 (kg)	Derivative Value		Wgt. #2 (kg)	Derivative Value		
16000	1100	x_u	-0.024111832	1300	x_u	-0.020953733	Stability Derivatives
		x_w	0.15237635		x_w	0.156406384	
		x_q	0		x_q	0	
		x_θ	-9.81		x_θ	-9.81	
		z_u	-0.304980779		z_u	-0.313199368	
		z_w	-0.051579548		z_w	-0.043919595	
		z_q	64.99424175		z_q	64.99457485	
		z_θ	0		z_θ	0	
		m_u	1.0794E-05		m_u	3.13472E-05	
		m_w	-0.025099251		m_w	-0.021234977	
		m_q	-0.066471045		m_q	-0.056244823	
		m_θ	0		m_θ	0	
		x_η	2.02642E-05		x_η	8.05432E-06	Control Derivatives
		x_τ	0		x_τ	0	
		z_η	-0.028641587		z_η	-0.024234999	
		z_τ	0		z_τ	0	
		m_η	0.251241533		m_η	0.212590557	
		m_τ	0		m_τ	0	

Source: Author's Documentation (2024)

RESULTS AND DISCUSSION

The longitudinal static and dynamic stability of the UAV has been studied, and several notes are worth mentioning. The UAV is generally dynamically stable when a small perturbation is initiated into the system. However, there is a concern regarding the time required for the UAV to reach the new equilibrium state after the perturbation has stopped, especially for the axial velocity response.

Longitudinal Static Stability

The UAV's static longitudinal stability describes its tendency to converge in the initial equilibrium following a small disturbance from the trim condition. The UAV is statically stable, and this is shown in one of the obtained derivatives, [M_w], which expresses pitch stiffness. The negative value of this derivative indicates the stable characteristic.

The derivative is dependent on the location of the static margin. A change in the location of the static margin will affect the stability of the UAV. The illustration in Figure 6 can depict the attitude of aircraft in general. For the current study, the negative value of indicates that the UAV has a negative moment with a static margin shaped by the location of the center of pressure behind the center of gravity.

However, longitudinal stability also discusses dynamic characteristics. While is also responsible for dynamic stability, other derivatives are not less important. Thus, there is a possibility that the UAV is statically stable but dynamically unstable. The evaluation of dynamic stability will be discussed further on the following page.

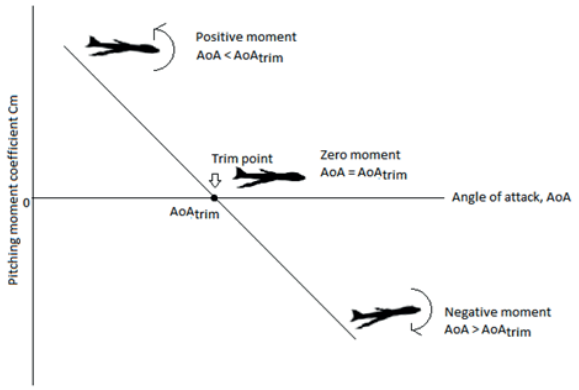

Figure 6.
Longitudinal Static Stability Moments as a Function of Angle of Attack
Source: Research Centre for Aeronautics Technology (BRIN) (2021)

Axial Velocity Response

Figure 7 shows that even though the UAV stabilizes, the time required to reach a new equilibrium still needs to be achieved 100 seconds after the perturbation is initiated. From this figure, the damping effect is not strong enough to subdue the effect of the perturbation in both the short period and phugoid modes. The effect of mass and inertia affect the width of the oscillation period, especially in the first 50 seconds.

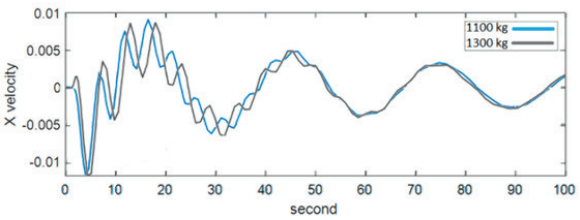

Figure 7.
Axial Velocity Response After an Arbitrary Perturbation
Source: Author's Documentation (2024)

The effect of aeroelastic deformation and compressibility contributes to the axial speed response. However, in the first place, the component of aeroelastic deformation has been ruled out from the stability derivative calculation. However, the compressibility effect is also minimal when the UAV is flying in the subsonic region, w, which can be concluded from the values of derivative being close to zero. This leaves the explanation of this trend shown in the figure as related to drag production due to the alteration of pitch angle, which will be discussed later.

Normal Velocity Response

In Figure 8, the response in normal velocity is shown. Similar to the axial velocity, the normal velocity response is influenced by phugoid mode. The new equilibrium is only partially achieved in 100 seconds, even though it is more dampened than the axial velocity. In the case of a weight of 1300 kg, the effect of inertia endorses a wider oscillation period, which is more manifest between 15 and 50 seconds. From this condition, a smoother transition towards new equilibrium is given by the weight of 1300 kg compared to 1100 kg. The change of angle of attack due to the perturbation, which is related to pitch angle, is responsible for the trend.

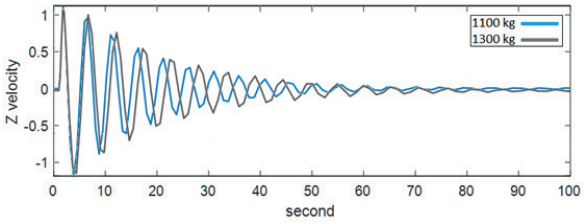

Figure 8.
Normal Velocity Response After an Arbitrary Perturbation
Source: Author's Documentation (2024)

There is a difference in how the response starts between axial velocity and average velocity trends. As the perturbation is initiated, the axial velocity tends to decrease, which can be explained as the perturbation has broken the airflow and induced the growth of drag. Conversely, the doublet given to the elevator has changed the value of the velocity component in the expected direction; hence, the trend is initiated similarly to the given perturbation.

Pitch Angle and Pitch Rate

In Figure 9, it can be seen that the figures for pitch rate and pitch angle responses are similar to the average velocity response. However, the new equilibrium of both parameters

has been reached in about 65 seconds, much faster than the axial and average velocity.

On many occasions, short-term response characteristics are necessary, mainly contributed by the short-period mode. The mode in the trim condition is mainly affected by the average velocity and pitch rate. Conversely, the axial velocity and pitch angle mainly affect the phugoid mode. The phugoid itself is rarely required in flight dynamics analysis as the response is usually weaker than the short period. However, the phugoid helps determine the UAV's efficiency as it is nearly proportional to the ratio. One seeks small values of this ratio to ensure the aircraft is efficient. Comparing the desired to the current occurrence, we may conclude that the UAV is ineffective enough to get a new stable condition after a given perturbation despite latent stability.

The issue may be tackled from at least two points of view. The first is revisiting aerodynamic design and proposing improvements to stimulate stability. The second one is to develop a control system that overcomes the issue. The extended consequence is the need for constant interference of the pilot or autopilot device to help correct the aircraft response after perturbation.

Flying Handling Qualities

The stability characteristics shown by the previously discussed figures are condensed in the solution of Laplace equations for all cases, along with the natural frequencies and damping ratios of each mode, as shown in Table 3. While there is no specific requirement, as the UAV cruising varies, the value should be predetermined and not be too small. In this current occurrence, the value is relatively small. However, the smaller value shows the more peculiar aspect; hence, underdamped oscillations are observed.

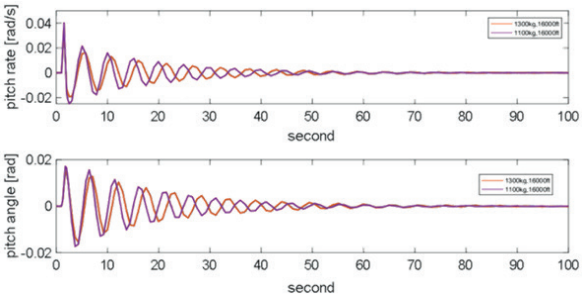

Figure 9.
Pitch Angle Response After an Arbitrary Perturbation
Source: Author's Documentation (2024)

The effect of weight manifests in the natural frequency and damping ratio in short-period mode. The case of 1300 kg gives less values in both natural frequency and damping ratio than 1100 kg. The more significant natural frequency causes the narrower gaps in the oscillation period. The effect of the damping ratio is related to the time needed to dampen the oscillation. Thus, the case of 1300 kg reaches the new equilibrium in a slightly longer time.

Table 3.
Eigenvalues of the system for different weight

Weight (kg)	Mode	
	Short Period	Phugoid
1100	-0.026643407 ± 1.27210388i ω_{sp} = 1.277329239 ς_{sp} = 0.020858684	-0.011931953 ± 0.198971289i ω_{ph} = 0.213437462 ς_{ph} = 0.055903741
1300	-0.022544421 ± 1.170165376i ω_{sp} = 1.174972008 ς_{sp} = 0.019187198	-0.010096966 ± 0.201263676i ω_{ph} = 0.213437462 ς_{ph} = 0.04730644

Source: Author's Documentation (2024)

The longitudinal stability characteristics shown by the UAV may affect the UAS's mission. In an intelligence, surveillance, or reconnaissance mission, it is imperative to obtain appropriate data. Suppose a small disturbance substantially affects the UAV's flying quality. In that case, it will cost the mission-related data transmitted to the ground station in both accuracy and precision matters. This condition, of course, can be handled with the current photogrammetry technology, but some premeditated arrangements need to be considered.

Even though there is no requirement for the UAV to have a specific natural frequency, especially in phugoid mode, ride quality is still important as it affects the effectiveness of the airframe. Although the phugoid effect requires less consideration, it may still increase the pilot's workload to carry out correction if the UAV is difficult or needs a considerable amount of time to stabilize.

CONCLUSION

The longitudinal dynamic stability analysis of the UAV is discussed. The stability derivatives of the UAV are obtained through wind tunnel data acquisition. The derivatives are evaluated, and the longitudinal motion characteristics are investigated by varying the weight of the UAV. It shows that the UAV tends to stabilize in static and dynamic stability. Stability characteristics have an essential role in carrying out the mission appropriately.

The main concern is the time needed to achieve stable conditions after an arbitrary perturbation is given. The axial velocity response is the most extreme, which is nearly undamped or highly underdamped. This is proven in the small value of short period and phugoid damping ratios. In two cases of 1300 kg and 1100 kg, the short period damping ratios are 0.019187198 and 0.020858684, respectively. As for the phugoid mode, the damping ratios are 0.055903741 for the case of 1100 kg weight and 0.04730644 for the case of 1300 kg weight. The smaller values of the short period damping mode are to be blamed for the UAV reaching a new equilibrium state after giving a small perturbation.

The effect of weight is apparent in the short-period mode, most notably with the short-period natural frequency. In the case of 1300 kg, the frequency is less than what is shown in the case of 1100 kg. Hence, the transition of the UAV towards a new equilibrium state is much smoother in the case of 1300 kg. The longitudinal stability characteristics influence the flying quality and appointed mission. The characteristics determine how the control system will be developed, and which technology will be installed in the system to achieve successful missions. They may also affect a pilot's handling quality during a flight.

Acknowledgements

This work is supported by the project "Dynamic Modelling of MALE UAV," Project ID: F.10, stipulated in Letter No.6/III/H.K./2022, and "Flight Control Computer Development of Upper 200 Kg UAV", Project ID: CFC.03; stipulated in Letter No.1/III.1/H.K./2023 under the grant of the Research Organization for Aeronautics and Space of National Research and Innovation Agency (BRIN) in Indonesia.

BIBLIOGRAPHY

Adeleke, O.A., Abbe, G.E., Jemitola, P.O. and Thomas, S. (2022). Design of the wing of a medium altitude long endurance UAV. International Journal of Engineering and Manufacturing (IJEM), 12(1), pp.37-47. https://doi.org/10.5815/ijem.2022.01.04

Adhynugraha, M.I., Budiarti, D.H., Muliadi, J., Nami, O.F., Octaviany, S.V. and Megawanto, F.C. (2023). December. Effect of tail and ruddervator on aerodynamics of UAV through wind tunnel study. In AIP Conference Proceedings (Vol. 2941, No. 1). AIP Publishing. https://doi.org/10.1063/5.0181637

Colomina, I. and Molina, P. (2014). Unmanned aerial systems for photogrammetry and remote sensing: A review. ISPRS Journal of Photogrammetry and Remote Sensing. Remote Sens. 92, 79–97. https://doi.org/10.1016/j.isprsjprs.2014.02.013

Cook, M.V. (2007). Flight Dynamics Principles. Book: Flight Dynamics Principles. https://doi.org/10.1016/B978-0-7506-6927-6.X5000-4

Gertler, J. (2012). U.S. unmanned aerial systems. Unmanned Aerial Systems (UAS). Drones Blimps 1–50.

Hasim, F., Rusyadi, R., Surya, W.I., Asrar, W., Omar, A.A., Mohamed Ali, J.S. and Kafafy, R., (2008). December. The IIUM low speed wind tunnel. In Proceedings of the 2nd Engineering Conference on Sustainable Engineering Infrastructures Development & Management (EnCon2008).

Henry, J., Blondeau, J., and Pines, D. (2005). Stability Analysis for UAVs with a Variable Aspect Ratio Wing. 46th AIAA/ASME/ASCE/AHS/ASC Structures, Structural Dynamics and Materials Conference. https://doi.org/10.2514/6.2005-2044

Iqbal, L., Crossley, W., Weisshaar, T., Sullivan, J. (2008). Higher Level Design Methods Applied to the Conceptual Design of an MALE UAV. 12th AIAA/ISSMO Multidisciplinary Analysis and Optimization Conference. https://doi.org/10.2514/6.2008-5908

Iqbal, L., Sullivan, J. (2009). Comprehensive Aircraft Preliminary Design Methodology Applied to the Design of MALE UAV, 47th AIAA Aerospace Sciences Meeting including the New Horizons Forum and Aerospace Exposition. https://doi.org/10.2514/6.2009-431

Li, X. and Savkin, A. (2021). Networked Unmanned Aerial Vehicles for Surveillance and Monitoring: A Survey. Futur. Internet 13, 174. https://doi.org/10.3390/fi13070174

O'Donnell, R. and Mohseni, K. (2018). Aerodynamic parameter estimation from wind tunnel testing of a small UAS. AIAA Atmospheric Flight Mechanics Conference. https://doi.org/10.2514/6.2018-0294

Panagiotou, P, Fotiadis-Karras, S., and Yakinthos, K. (2018). Conceptual design of a Blended Wing Body MALE UAV. Aerospace Science and Technology. 73, 32–47. https://doi.org/https://doi.org/10.1016/j.ast.2017.11.032

Panagiotou, P., Kaparos, P., Salpingidou, C., and Yakinthos, K. (2016). Aerodynamic design of a MALE UAV. Aerospace Science and Technology. 50. https://doi.org/10.1016/j.ast.2015.12.033

Panagiotou, Pericles, Giannakis, E., Savaidis, G., and Yakinthos, K. (2018). Aerodynamic and structural design for the development of a MALE UAV. Aircraft Engineering and Aerospace Technology. 90. https://doi.org/10.1108/AEAT-01-2017-0031

Paper ICAS-98-3.11.3

Purwadi, P. (2019). Peran Laboratorium Pengujian Aerodinamika Pada Percepatan Kemandirian Bangsa. Prosiding SENIATI, 5(1), pp.370-376. https://doi.org/10.36040/seniati.v5i1.465

Purwadi, P., Hidayat, A.R., Hariz, I., Satriya, I.A.A., Kuswandi, K., Triwulandari, R. and Pinindriya, S.T. (2023). December. Designing of hinge moment balance for hinge rudder performance measurement in Indonesian low speed tunnel (ILST). In AIP Conference Proceedings

(Vol. 2941, No. 1). AIP Publishing. https://doi.org/10.1063/5.0181422

Sakya, A.E., Wiriadidjaja, S. and Adibroto, A. (1998). Commemorating Ten Years Operation Of The Indonesian Low Speed Tunnel (ILST). 21st Congress of International Council of the Aeronautical Sciences, Melbourne, Australia, 13-18 September, 1998

Soemaryanto, A.R., Herdiana, D., Wahyudi, W., Triwulandari, R. and Aziz, M.N. (2023). December. Parametric study of extended horizontal tailplane of commuter aircraft using wind tunnel testing. In AIP Conference Proceedings (Vol. 2941, No. 1). AIP Publishing. https://doi.org/10.1063/5.0181442

Stodola, P., Drozd, J., Mazal, J., Hodicky, J., and Prochazka, D. (2019). Cooperative Unmanned Aerial System Reconnaissance in a Complex Urban Environment and Uneven Terrain. Sensors 19, 3754. https://doi.org/10.3390/s19173754

Taylor, D. (2010). Marine: Demand "beginning to boil": ONR Meets With Industry For Long-Term Cargo UAS Program In Mid-2010s. Insid. Navy 23, 1–12.

Wienke, F., Raffel, M., and Dillmann, A. (2021). Wind Tunnel Testing of Otto Lilienthal's Production Aircraft from 1893. American Institute of Aeronautics and Astronautics (AIAA) Journal. 59, 1342–1351.